Rasool Ghobadian
Associate Professor
Department of Water Engineering,
Razi University, Kermanshah, Iran
rsghobadian@gmail.com

Dejana Djordjevic
Assistant Professor
Department of Hydraulic and Environmental Engineering, Faculty of Civil Engineering, University of Belgrade, Belgrade, Serbia
dejana@grf.bg.ac.rs

Masha Basiri
PhD. Student
Department of Water Engineering,
Razi University, Kermanshah, Iran
basirimahsa@yahoo.com

ASSESSMENT OF THE IMPACT OF BEND TYPE ON FLOW CHARACTERISTICS IN 180° COMPOUND BENDS

River bends are rarely simple, i.e., the bend radius is rarely constant throughout the bend length. They are rather irregular, i.e. their shape in the plan can be approximated with different bend radii. Since the bulk of previous research is concerned with simple bends, this paper aims at studying the effect of variable bend curvature on flow in an irregular bend with two bend radii. The effect is studied numerically, using a 3D finite volume based model SSIIM1, which solves Reynolds-Averaged Navier-Stokes (RANS) equations with two-equation turbulence model closure. After successful calibration against experimental data from the simple 180° bend, the model is used to simulate flow in 180° variable curvature bends with the following combinations of relative curvature: mild-mild, mild-sharp and sharp-mild. Results have shown that: (1) The maximum spanwise water surface slope always develops at the entrance to the sharp bend, (2) the greatest slope develops in the sharp-mild layout, (3) the location where the maximum velocity path cuts the bend centerline does not change with the bend layout (simple or variable curvature), (4) the bend curvature sequence affects lateral velocity distributions of the streamwise velocity only in the middle of the bend, (5) the relative curvature sequence has an adverse effect on the size of two regions with maximum bed shear stress – one around the curvature inflection point and the other close to the bend exit.

Keywords: Variable Curvature Bend, Relative Curvature, Shear Stress, SSIIM1

1. INTRODUCTION

River channels are rarely straight. Even in straight reaches the thalweg meanders. Artificial channels (irrigation, drainage and navigation canals) also have bends. They are usually forced by various constraints (design, topographic, etc.). River bends are rarely simple, i.e., they rarely have a constant radius throughout their length. They rather have variable curvature, which means that their shape in the plan view can be described with several different radii. There are many studies

of flow in river bends ([5-8], [10,11], [15], [33], [25], [27], [19], [39], [2], [23], [38]). Further, the flow in bends is three-dimensional and the hydrodynamics of bends in movable bed channels is very complex due to scour and deposition in different parts of the bend. The rate of erosion in a bend depends on the flow properties, sediment composition of river/ channel banks and the channel geometry [4]. Rozovskii [31] classified bends into sharp and mild bends, depending on the value of the radius to width ratio (R / W), i.e., relative curvature (where R is the radius of the bend centreline and W is the channel width). According to Rozovskii's classification, the R / W-value in sharp bend is less than 3.0 and for mild bends, it is larger than 3.0. One of the early studies on the bend flow hydrodynamics was conducted by Shukry [34]. This study reports experimental results from 90° and 180° open channel bends in channels with rectangular cross section and different values of radius to width ratio. The effect of the bend was investigated under different Reynolds numbers, depth-to-width and radius-to-width ratios. Rozovskii [4] studied flow characteristics and boundary shear stress distribution in channel bends. Mosonyi and Gotz [22] investigated the secondary flow pattern and helical flow strength in bends. Their results showed that the secondary flow can be well described by changes in its strength. Leschziner and Rodi [17] presented a three-dimensional numerical model based on the finite-difference method for simulation of turbulent flow in strongly curved channels with rectangular cross-section. They studied the effect of the streamwise pressure gradient on the flow pattern in swift bends. Manssori [21] studied the sedimentation and scouring pattern in a 180° open channel bend using SSIIM model. The computed bed profiles clearly indicated development of a point bar and a pool in two regions within the bend – the first one was positioned close to the location defined by the central angle $\theta = 45°$ and the second one close to $\theta = 130°$. Fazeli et al. [12] carried out an experimental study in a 90° open channel mild bend. They studied the effect of a spur dike on flow and scouring patterns and presented an equation for the estimation of a maximum scour depth. Ahmadi et al. [1] proposed a 2D depth-averaged model for the simulation of unsteady flow in open channel bends. The comparison of the simulation results and the experimental data has shown good agreement between predicted and measured water surface profiles in both sharp and mild bends. Stoesser et al. [35] studied numerically 3D flow and wall shear stress distributions in a meandering open channel by using the Large Eddy Simulation approach and a method that is based on Reynolds-Averaged Navier-Stokes (RANS) equations for which two different isotropic turbulence closures were employed. Their overall results indicated that the predicted bed-shear stresses in RANS simulations is about 15-20% higher than that in the LES, particularly in the centre of the channel at the entrance and the exit sections of the bend as well as near the inner bank at the apex. Results also provide clear evidence that the RANS code is able to predict time-averaged primary velocities which are in good agreement with measurements regardless of the turbulence model used. LES was found to be slightly superior to RANS in computing the time-averaged secondary velocities. Esfahani and Keshavarz [10] studied the effect of different curvatures inside the river meander on flow characteristics in a bend. Two physical models of river meander with different curvature were studied. Each model consisted of three sequential bends. Results showed that the effect of the centripetal force of preceding and succeeding bends on the tangential velocity, bed topography and flow structure in the middle, second bend was stronger in the model 1 with sharp multi bend than in the model 2 with mild multi bend. Blanckaert [5] studied secondary flow saturation, outer banks cells and inner bank flow separation of sharp bends with fixed banks and discussed their morphological effects. Ghobadian and Mohammadi [13] carried out a numerical study in 180° uniform and convergent open channel bends using SSIIM model. Their results have shown that the maximum velocity path near the water surface crossed the channel's centreline in the cross-section located between $\theta = 30°$ and $\theta = 40°$ for convergent channel, while in the uniform bend, the crossing was located at $\theta = 50°$. Vaghefi et al. [37] carried out an experimental study in a 90° bend and investigated the effect of Froude number on scouring depths around a T-shaped spur dike. Their results showed that two scour holes developed due to a presence of the T shaped spur dike – one at the nose of the spur dike and the other one downstream of the dike. Liyaghat et al. [20] investigated the effect of increasing and decreasing width of a 180° bend on flow characteristics in a bend. They calibrated the model for a uniform bend and then compared flow patterns with those in divergent and convergent bends. Results showed that in the convergent bend the maximum velocity path near the water surface crossed the channel's centreline between $\theta = 30°$ and $\theta = 40°$. In the divergent bend the crossing was close to $\theta = 50°$, whereas in the bend with uniform channel width, the crossing was located around $\theta = 55°$. Vaghefi et al. [36] conducted an experimental study on

flow velocity components in a 180° sharp bend. The results showed that the maximum velocity occurred at the inner bank of bend due to strong pressure gradients at the bend entrance. The results also indicated that the values of the vertical velocity component at the bend entrance were positive near the bed and adjacent to the inner wall and negative in other areas.

This review shows that the previous work was primarily focused on simple bends and that the flow pattern in variable curvature bends was rarely studied. The previous work (e.g., [3], [18], [14], [24]) has also indicated that sharp bends' hydrodynamics differs from that in mild curvature bends. Additionally, the hydrodynamics in case of different combinations of sharp and mild bends may differ from those for single bends with moderate and sharp curvature. Thus, this paper aims at assessing the effect of different combinations of bend curvature sequences on flow and bed shear stress patterns in a 180° variable curvature bend. The effect is studied using a 3D finite volume based model SSIIM1. The model is calibrated first against the experimental data from a simple, mild bend. Consequently, three layouts of a variable curvature bend are analysed: "Mild-Mild", "Mild-Sharp" and "Sharp-Mild". The "Mild-Mild" layout has two mild bends with $R / W = 5$ in the first bend and $R / W = 3.67$ in the second one. The R / W ratios in the leading and the secondary bends of the "Mild-Sharp" layout are 5.83 and 2.83, respectively, whereas the corresponding ones of the "Sharp-Mild" bends are 2.83 and 5.83. The effect of different variable curvature bend layouts is studied by comparison of: (1) water surface profiles along the inner and outer banks, (2) maximum velocity paths close to the free-surface, (3) lateral profiles of the streamwise velocity in different cross-sections within the bend and (4) bed shear stress distributions with the corresponding ones in the simple bend.

2. MATHEMATICAL MODEL

2.1 GOVERNING EQUATIONS

The three-dimensional steady incompressible fluid flow is described by the mass conservation and Reynolds-Averaged Navier-Stockes (*RANS)* equations [28]:

$$\frac{\partial U_j}{\partial x_j} = 0, \quad j = 1, 2, 3 \tag{1}$$

$$\frac{\partial U_i}{\partial t} + U_j \frac{\partial U_i}{\partial x_j} = \frac{1}{\rho} \frac{\partial}{\partial x_j} \left(-P\delta_{ij} - \rho \overline{u_i' u_j'} \right) \tag{2}$$

In these equations time t and space coordinates x_j, $j = 1, 2, 3$ are independent variables. Dependent variables are: time averaged velocities in the three coordinate directions U_j, $j = 1, 2, 3$, the time averaged pressure P, and Reynolds stress terms $\rho \overline{u_i' u_j'}$, $i, j = 1, 2, 3$. The density of water is denoted by ρ and the symbol δ_{ij} is the Kronecker delta. The Kronecker δ_{ij} is equal to 1 if $i = j$, and it is equal to 0 otherwise. The last term, which describes the contribution of velocity fluctuations u_i' and u_j' to the flow of momentum in the j-direction, i.e. the Reynolds stress term, is modelled with the Boussinesque approximation [28]:

$$\rho \overline{u_i' u_j'} = \rho \nu_t \left(\frac{\partial U_i}{\partial x_j} + \frac{\partial U_j}{\partial x_i} \right) - \frac{2}{3} \rho k \delta_{ij} \tag{3}$$

where ν_t is the eddy viscosity and k is the turbulence kinetic energy (*TKE*). The eddy viscosity is not a fluid property, but strongly depends on the state of turbulence and can be determined using turbulence models with different levels of complexity: zero-equation models, one-equation models or two-equation models as described in [30]. In two-equation models the eddy viscosity is a function of the turbulence kinetic energy k and turbulence dissipation rate ε as described by Kolmogorov-Prandtl equation [30]:

$$\nu_t = C_\mu' \frac{k^2}{\varepsilon} \tag{4}$$

The turbulence kinetic energy k is defined as:

$$k = \frac{1}{2} \overline{u_i' u_j'} \tag{5}$$

The transport equation of k is the same for the standard and *RNG* types of *k*-ε turbulence model [30]:

$$U_i \frac{\partial k}{\partial x_i} = \frac{\partial}{\partial x_i} \left(\frac{\nu_t}{\sigma_k} \frac{\partial k}{\partial x_i} \right) - \\ - \nu_t \left(\frac{\partial U_i}{\partial x_j} + \frac{\partial U_j}{\partial x_i} \right) \frac{\partial U_i}{\partial x_j} \tag{6}$$

The general form of the transport equation for ε is described by the following expression [30]:

$$U_i \frac{\partial \varepsilon}{\partial x_i} = \frac{\partial}{\partial x_i} \left(\frac{\nu_t}{\sigma_\varepsilon} \frac{\partial \varepsilon}{\partial x_i} \right) - C_{1\varepsilon} \frac{\varepsilon}{k} P_k - \\ - C_{1\varepsilon} \frac{\varepsilon^2}{k} - \alpha \frac{\varepsilon^2}{k} \tag{7}$$

The last term is an extra term and describes the influence of small-scale vortices (smaller than the grid size) that are developed during the *TKE* dissipation in shear flows. This is the mean strain rate, which accelerates turbulence dissipation in

areas with the increased shear. The turbulence model parameters have the following values: C'_μ = 0.09, σ_k = 1.00, σ_ε = 1,30, $C_{1\varepsilon}$ = 1.44, $C_{2\varepsilon}$= 1.92. These are the default values in the SSIIM1 for the k- ε turbulence model. The extra term contains a parameter α, which is defined by the ratio η of two time scales – that of the turbulent strain and that of the mean strain. Expressions for α and η read:

$$\alpha = C'_\mu \eta^3 \frac{(1-\eta/\eta_0)}{1+\beta\eta^3}, \qquad \eta = S\,\frac{k}{\varepsilon}, \qquad S = \sqrt{2\,S_{ij}^2} \qquad S_{ij} = 0.5\left(\frac{\partial U_i}{\partial x_j} + \frac{\partial U_j}{\partial x_i}\right) \tag{8}$$

In these expressions η_0 is a fixed point for homogeneously strain turbulent flows (η_0 = 4.8) and β = 0.12. Thus, when the mean strain is weak ($\eta \to 0$), the extra production term is also small, but when the mean strain rate is strong (large η), the extra production term leads to an increase in turbulence dissipation. Consequently, the eddy viscosity is decreased and the momentum of the mean flow is reduced. The resulting recirculation zone size is comparable to that observed in laboratory experiments.

Boundary Conditions

The full description of the problem requires that the governing equations are supplemented with boundary conditions. Boundary conditions are defined at open and solid boundaries. Open boundaries include inflow and outflow cross-sections and the free-surface, whereas solid boundaries include channel bed and walls/banks.

Inflow and Outflow Boundaries

Dirichlet boundary condition is applied at the inflow boundary. The application of this condition is relatively straightforward for velocities. However, it is more difficult to specify the turbulence properties, i.e. k and ε. Their values are found from: 1) the distribution of the eddy viscosity coefficient (ν_t = 0.11u_*h, [16]) or the depth averaged value ν_t = 0.067u_*h) the assumption that the production and the dissipation of the *TKE* are at equilibrium near the solid boundary and 3) the assumption of the linear distribution of the *TKE* in which the free-surface value is equal to half of its bottom values [26]. For the given velocity, it is also possible to estimate the bed shear stress (τ), which can be further used to find the *TKE* value on the bed in the inflow cross-section:

$$k = \frac{\tau}{\rho\sqrt{C'_\mu}} \tag{9}$$

Based on the previously determined values of the eddy viscosity and *TKE* on the bed, the corresponding value of the *TKE* dissipation rate ε can be found using the equation (4). The vertical profile ε (x_3) is then calculated based on the ν_t and *k* vertical profiles.

Water Surface

The free surface is computed using a fixed-lid approach, with zero gradients for all variables except the vertical velocity which is calculated from the zero discharge condition through the free-surface, and the *TKE*, which is set to half of its bottom value, as already described. The location of the free-surface is determined from the calculated pressure field using Bernoulli equation.

Solid Boundaries - bed/wall

The wall-law for rough boundaries was used as a boundary condition for the bed and wall [32]:

$$\frac{U}{u_*} = \frac{1}{\kappa}\ln\frac{30\,y}{k_s} \tag{10}$$

Here, the bed effective roughness is denoted with the symbol k_s. The bed effective roughness after van Rijn is used in this study. Other variables in Eq. 10 include velocity U, shear velocity u_*, von Karman constant κ = 0.4 and the distance from the wall to the centre of the first computational cell *y*.

2.2 NUMERICAL MODEL

The set of six equations (1), (2), (6) and (7) is solved on a structured, curvilinear, orthogonal space grid using a 3D finite-volume model SSIIM1. Convective terms in the momentum equations can be discretized either using the power-law or the second-order upwind scheme. In this paper the power-law scheme is used. Since the velocity field, which is obtained by solving *RANS* equations (2), does not satisfy the mass conservation equation (1), the coupling of equations is achieved using the SIMPLE algorithm [26]. Velocity derivatives in transport equations for *TKE* and ε are discretized using central differences.

2.3 EXPERIMENTAL SETUP

Prior to the study of the effect of a variable curvature bend layout on the flow characteristics in the bend, the selected numerical model (SSIIM1) is calibrated against the experimental data from a 180º simple bend with a constant

Figure 1. Pirestani's experimental facility (Pirestani, 2004)

bend radius [29]. The data were collected in a laboratory flume made in the Tarbiatmodarres University Laboratory with the bend of radius R = 2.6 m which was inserted between two straight channels (Fig. 1). The length of the upstream channel is 7.2 m and that of the downstream channel is 5.2 m. The cross-section of the flume is a square with a 0.6 m long edge. This gives a radius to width ratio-value R / W = 4.33. A bend with this R / W value belongs to the class of mild bends according to Rozovskii [31] classification. The longitudinal channel bed slope is 0.0015.

Experiments were carried out for three discharge values Q = {30, 45, 60} l/s and three Froude number values Fr = {0.27, 0.41, 0.55}. The discharge was measured on the calibrated orifice set in the supply pipe, while longitudinal and lateral velocity components were measured using the P-EMS velocimeter. A digital point gauge with an accuracy of ±0.01 mm was used for flow depth measurements. Pirestani's data from the experiment with the constant discharge of 30 l/s and the flow depth of 0.15 m at the entrance to the channel were used for verification of the numerical model.

2.4 VERIFICATION OF THE NUMERICAL MODEL

The computational domain covered the full length of Pirestani's facility to ensure no influence of boundary conditions on the flow pattern in the bend (Fig. 2). Since

SSIIM1 grid generator can make only uniform grid, an independent mesh generator was written in Visual Basic to produce a desired non-uniform grid with higher cell density near channel walls (Fig. 3a). In addition to lateral, it is also possible to provide longitudinal cell-size variabilty. This allows one to reduce computational time by increasing the cell length in the streamwise direction along the upstream and downstream straight reaches, which are of no interest for the present study.

A special attention was paid to grid sensitivity analysis and model calibration, since the model output is strongly affected by the grid size/ density, imposed boundary conditions and wall roughness. All three were varied until acceptable match has been attained between simulated and measured water surface profiles, pressures and velocities. Statistical indicators such as $RMSE$ (root-mean-square error) and MAE (mean absolute error) were used to assess the quality of the SSIIM1 model results:

$$RMSE = \sqrt{\frac{1}{N}\sum_{i=1}^{N}[\,(U_c)_i - (U_m)_i\,]^2} \qquad (11)$$

$$MAE = \frac{1}{N}\sum_{i=1}^{N}[\,(U_c)_i - (U_m)_i\,] \qquad (12)$$

Here the subscript m refers to the measured variable value and c to the calculated one. To select the final mesh size, study of grid sensitivity analysis was done based on comparison of calculated water surface and streamwise flow velocity at different cross-sections with the measured ones. For this purpose, three mesh sizes were considered. The coarse mesh with size 71×12×7 in the streamwise, lateral and vertical directions, respectively, the fine mesh of 91×19×7 size and the finest mesh of size 351×35×15. The grid sensitivity analysis has shown that the mesh of size 91×19×7 provided satisfactory results. This means that the choice of a finer mesh has not significant effect on the quality of results when compared to the selected mesh size.

Lateral profiles of the streamwise velocity component (U) near the free-surface, that were obtained with the absolute roughness k_s = 0.1 mm and the downstream flow depth of 0.14 m

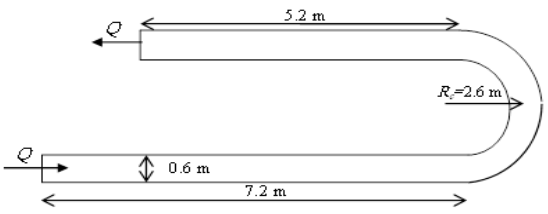

Figure 2. Dimensions of the computational domain in the plan view

are compared to measured ones in several cross-sections within the bend (Figs. 4, 5). Values of the $RMSE$ and MAE for the five cross-sections are given in Table 1. Low values of both statistics in all selected cross-sections clearly indicate that the SSIIM1 model gives physically plausible results with acceptable level of accuracy. Velocities are over predicted close to the bend entrance (θ = {10º, 40º}) by 0.028 and 0.039 m/s on the average, while the match between the two is almost perfect in the middle part (θ = {90º, 130º}), i.e. MAE = 0.015 m/s. Although a greater dispersion in measured elocities is observed at the exit (θ =170º), the shape of the lateral profile is caught satisfactorily.

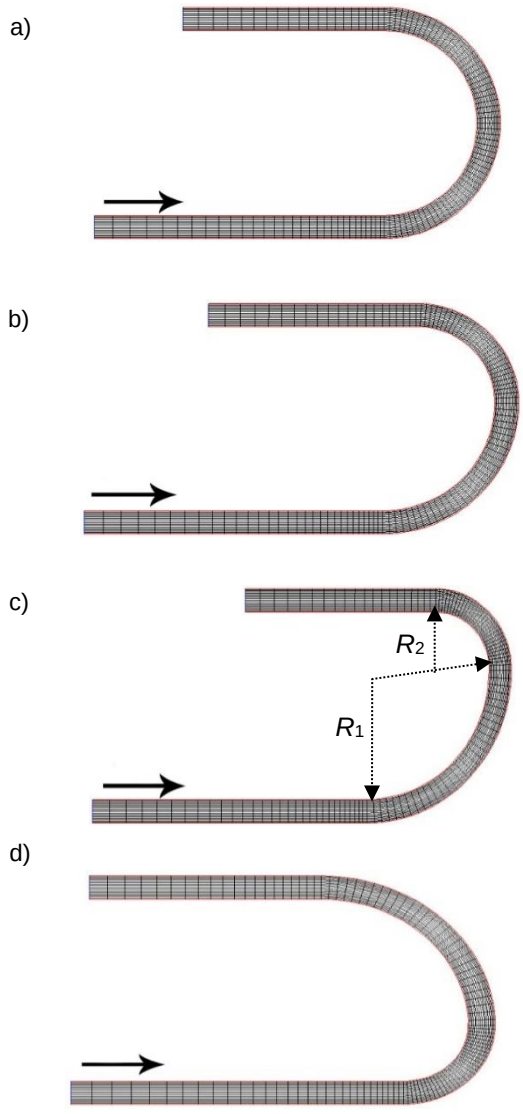

Figure 3. Schematic view of the generated mesh for: a) Simple, b) Mild-Mild, c) Mild-Sharp and d) Sharp-Mild bends

Table 1. Comparison of calculated and measured velocities in plane near water surface

Statistical indicators	Section location				
	10º	40º	90º	130º	170º
$RMSE$ [m/s]	0.0350	0.0457	0.0216	0.022	0.0315
MAE [m/s]	0.0285	0.0398	0.0152	0.0156	0.0276

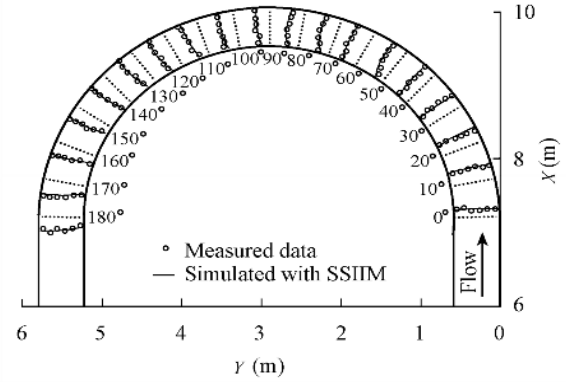

Figure 4. Comparison of streamwise velocity profiles on the plane near the water surface (circles are used for experimental data and lines for simulation results; dotted lines indicate position of profile lines), [13]

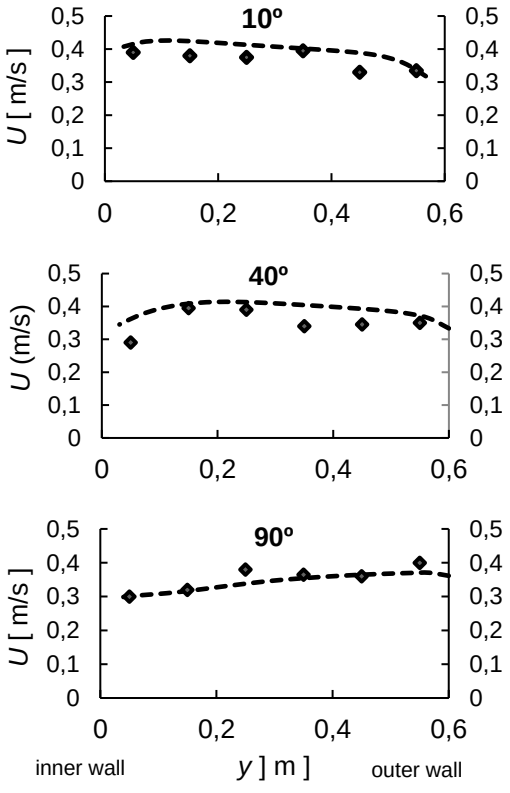

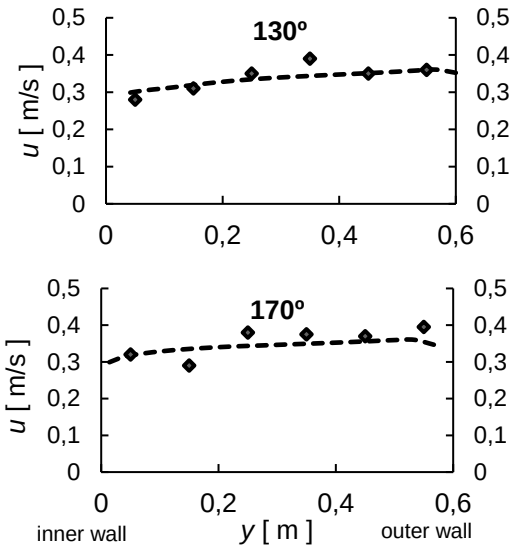

Figure 5. Comparison of calculated (dashed line) and measured (diamond-symbol) lateral profiles of the streamwise velocity within the bend (Profiles are presented on the plane near water surface)

In addition to streamwise velocity profiles on the plane near the water surface, simulated streamwise vertical profiles at the exit cross section of the bend are compared with the experimental ones. As it can be seen from Fig. 6, the model predictions only at the water surface and close to bed near the inner and the outer walls of the bend slightly deviate from the measured ones (relative error is less than 14.43%). In the middle of the cross-section (y = {0.5-0.45} m) the model predictions are relatively good (relative is error less than 11.28%).

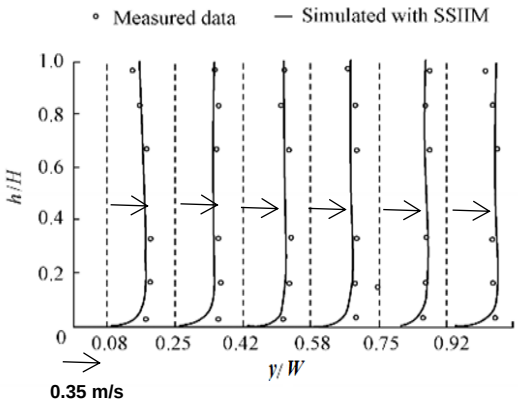

Figure 6. Comparison of the calculated vertical velocity profiles of the streamwise velocity with experimental data in the exit cross-section ω = 180º, [13]

2.5 NUMERICAL EXPERIMENTS IN A VARIABLE CURVATURE BEND

To study the effect of variable bend curvature ratio on flow characteristics in 180º bend, three hypothetical variable curvature bend layouts are considered (Table 2). They cover three possible cases: 1) case when both successive bends are of mild type, 2) case when mild bend precedes the sharp one and 3) case when sharp bend precedes the mild one. The cross-sectional channel geometry and lengths of the upstream and downstream straight channel sections are taken from Pirestani's facility (Fig. 2). Grid with the same size as the one used in the simple bend is applied in all hypothetical confluence layouts (Figs. 3b, c, d). To facilitate comparison with the simple bend case, numerical experiments were conducted with the same hydraulic data (see Section 3).

Table 2. Types of studied bends

Bend case (Fig.1)	R_1 [m]	R_1/W	R_2 [m]	R_2/W	Bend class	Bend type
a	2.6	4.33	2.6	4.33	Simple	Mild
b	3	5	2	3.33	variable curvature	Mild-Mild
c	3.5	5.83	1.7	2.83	variable curvature	Mild-Sharp
d	1.7	2.83	3.5	5.83	variable curvature	Sharp -Mild

3. RESULTS AND DISCUSSION

The effect of a variable curvature bend on flow characteristics in 180° bend is studied by comparison of: 1) the streamwise water surface profiles along the outer and inner banks, 2) maximum velocity paths, 3) lateral profiles of the streamwise velocity and 4) bed shear stress distributions for the four considered bend layouts.

3.1 EFFECT OF BEND TYPE ON STREAMWISE/SPANWISE WATER SURFACE PROFILES

Non-dimensional water surface profiles along the outer and inner banks for different bend layouts of a variable curvature bend are presented in Figure 7. Water surface profiles are non-dimensionalised using the flow depth at the outflow cross-section (h_d = 0.14 m). The distance along the channel L is non-dimensionalised using the total channel length L_t. The following can be observed. Water surface profile along the outer bank in the part of the variable curvature bend with the larger curvature (sharp bend) is always above the corresponding profile of the simple bend regardless the bend sequence (Sharp-Mild or

Mild-Sharp). This is expected since the centrifugal force in the bend with the greater curvature is stronger. As such, it produces greater water level rise along the outer bank. Conversely, the water surface profile along the inner bank of the sharp-bend reach in the variable curvature bend is always below that in the simple bend. Additionally, it is readily noticeable that the spanwise (lateral) water surface slope, which is present throughout the bend due to the difference in water surface elevations at the opposite banks, develops at a short distance upstream of the bend. This phenomenon is caused by the change in the direction of the streamwise momentum as the flow approaches and enters the bend [13].

As it can be seen from the water surface profiles of the Mild-Mild and the Mild-Sharp bends, the water surface elevations along the entrance section (L / L_t = 0.0 to 0.32) are lower than those along the same stretch of the simple bend when the compound bend begins with a bend that has greater radius than the simple bend. The situation is quite the opposite when the compound bend starts with the bend of smaller radius then the simple bend.

The spanwise water surface elevation difference from L / L_t = 0.32 (entrance to the bend) to L / L_t = 0.54 in the case *b* (Mild-Mild sequence of bends) is 8.9% smaller than the corresponding spanwise water surface elevation difference in the simple bend. From L / L_t = 0.54 till the end of the bend it becomes 50.1% greater than the corresponding spanwise water surface elevation difference in the simple bend. Such a behaviour is explained by the fact that the bend radius of a compound bend *b* is less than the radius of simple bend from L / L_t = 0.32 to L / L_t = 0.54 and it is greater from that of the simple bend from L / L_t = 0.54 to the exit of bend. Therefore, the centrifugal force in the first part of the bend in case *b* is smaller than that in the simple bend and it is greater than the corresponding one in the simple bend in the remaining part of the compound bend.

In the bend case *c* (Mild-Sharp bend), the spanwise water surface elevation difference is 17.2% less than that in the simple bend in the first part of the bend (L / L_t = 0.32 to 0.57) because the bend radius is larger than that in the simple bend. The bend radius in the second part of the compound bend is also less than that in a simple bend and it is smaller than that in the case *b*. Thus, the resulting spanwise water surface elevation difference is 72.74% larger than that in the simple bend.

In the bend case *d* (Sharp-Mild bend) the situation is the opposite to the bend case *c,* which means that the spanwise water surface elevation difference in the first part of the bend (sharp bend) is 46.24% greater than that in the simple bend while it is 22.21% less than that in the simple bend in the second part of the compound bend (mild bend).

There is almost no difference between the simple and compound bends' water surface profiles downstream of the bend (L / L_t = 0.75 to 1.00).

The maximum non-dimensional spanwise water surface elevation difference ($H_{max} = (h / h_d)_{max}$) and its location ($L_{Hmax} / L_t$) are listed in Table 3 (L_t is the total length of the computational domain). It is readily noticeable that the largest difference ($\max H_{max}$) develops in the Sharp-Mild bend at the location which matches that of the simple bend.

Changes in lateral water surface slope (S_l) in simple and compound bends are compared in Figure 8. One can notice that the Sharp-Mild compound bend layout produces the steepest lateral slope S_l = 0.56% at L / L_t = 0.37. This maximal slope is 80.64% greater than the maximal slope in the simple bend ($\max S_l$ = 0.31%). However, starting from L / L_t = 0.48 the lateral slope S_l for the Sharp-Mild bend becomes approximately 69% smaller than that in the simple bend. At the exit of the bend, it coincides with that of the simple bend. In both Mild-Mild and Mild-Sharp layouts, the maximal lateral slope in the upstream, Mild bend is smaller than that in the simple bend due to a smaller curvature. It is 19.3% smaller in the Mild-Mild and 32.2% smaller in the Mild-Sharp bend. Shortly after the change in bend curvature, the lateral slope becomes greater than that in the simple bend due to larger curvature of the second bend when compared to the simple one. The maximal lateral slope in the Sharp second bend (Mild-Sharp layout) is 26.6% greater than that in the Mild second bend of the

Table 3. Maximum spanwise water surface elevation difference and its location

Bend type	$H_{max} = (h/h_d)_{max}$	L_{Hmax}/L_t	$\max S_l$ [%]
Simple	0.0001879	0.383	0.31
Mild-Mild	0.0001407	0.597	0.26
Mild-Sharp	0.0001791	0.669	0.30
Sharp-Mild	0.0003347	0.383	0.56

Mild-Mild layout. The location of the maxS_l is shifted downstream by 0.23L_t in the Mild-Sharp when compared to the Mild –Mild bend. However, the slope reduction towards the bend exit is much slower than in the Mild-Mild layout.

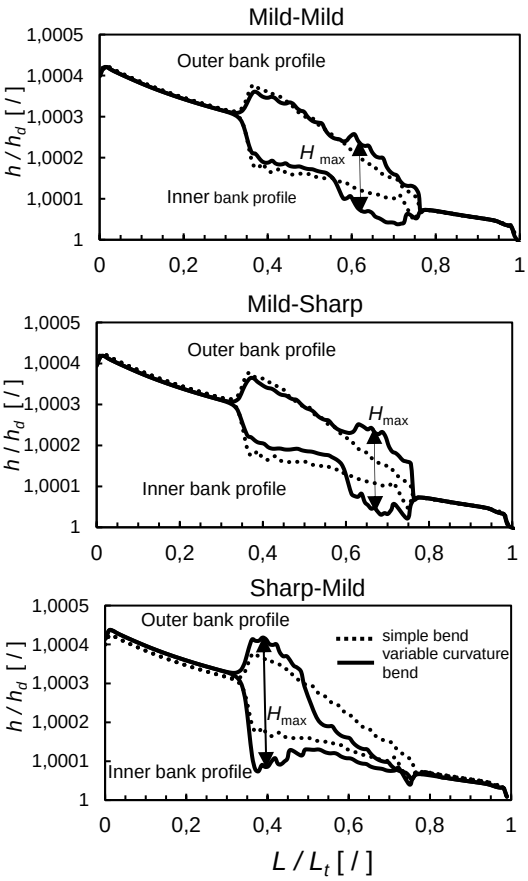

Figure 7. The effect of bend type on water surface profile (L is distance from beginning of channel, L_t is the total channel length and h / h_d is dimensionless water depth ratio

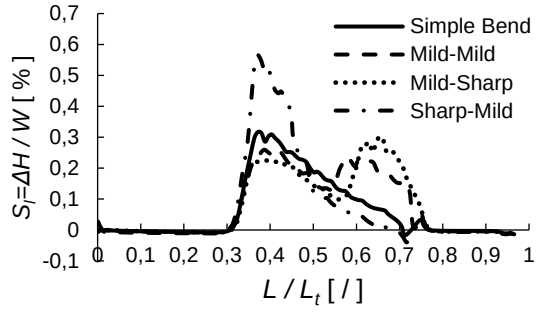

Figure 8. The effect of bend type on spanwise water surface slope

3.2 EFFECT OF BEND TYPE ON MAXIMUM VELOCITY PATH

The maximum velocity path is the line which connects points with maximum velocity magnitude at a given elevation above the bed. Figure 9 shows a schematic of the maximum velocity path near the water surface. Two points are indicated in this figure: the point L_1 where the maximum velocity path cuts the centreline and the point L_2 where it reaches the outer bank and from which it keeps following this bank. Distances of the two points from the beginning of the bend are also denoted by L_1 and L_2. These lengths are non-dimensionalised by the total length of the bend (L_b). They are presented in the Table 4. As can be seen, the maximum velocity path cuts the centreline at the shortest distance in the Mild-Sharp bend, which means that the influence of the centrifugal force in this compound bend layout increases much faster than in the other bend layouts. However, it can be concluded that the distance is practically the same regardless of the bend layout (variable curvature or simple) since the difference between the simple and variable curvature cases is 7% at maximum. On the other hand, the distance L_2 in the variable curvature bend is shortened when compared to the simple bend. The maximum shortening (27%) is recorded in the Sharp-Mild bend, which means that in this bend layout the secondary flow takes the dominance over the effect of streamwise pressure gradient much faster than in other considered layouts.

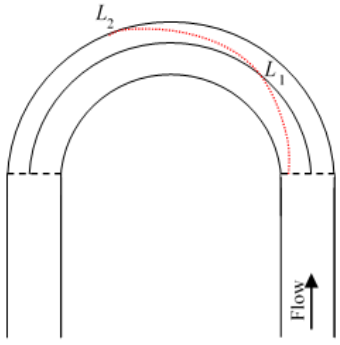

Fig. 9. Schematic image of maximum velocity path near the water surface

3.3 EFFECT OF BEND TYPE ON LATERAL PROFILES OF STREAMWISE VELOCITY

Lateral profiles of the streamwise velocity for different bend layouts are compared in Figure 10. The bend layout practically has no influence on lateral profiles at the entrance to the bend (L / L_b = 0.00) and close to its exit (L / L_b = 0.75).

Here L stands for the distance of the cross-section from the entrance to the bend measured along the path of maximum velocity, and L_b is the total length of the bend. The only visible differences are recorded near the inner and outer banks in the Sharp-Mild bend. The maximal increase in the velocity magnitude of 4.61% is recorded near the inner bank at $L / L_b = 0.00$ and the maximum decrease of 4.76% is recorded near the outer bank close to the bend exit ($L / L_b = 0.75$). Such behaviour becomes prominent for the opposite bend curvature sequence in the variable curvature bend, i.e. for the Mild-Sharp bend. Differences between the four distributions start to emerge from $L / L_b = 0.25$ and increase till $L / L_b = 0.50$. At $L / L_b = 0.25$ the lowest velocity magnitudes are recorded in the Sharp-Mild bend and the largest in the Mild-Sharp bend, with the remark that differences between the Simple, Mild-Mild and Mild-Sharp bends are practically negligible in this cross-section. In the middle of the bend ($L / L_b = 0.50$) velocity magnitudes in the Mild-Mild and Mild-Sharp bends are greater than in the Simple bend, while those in the Sharp-Mild bend remain the lowest. The maximum velocity difference of 10.18% between the Mild-Sharp and Sharp-Mild cases is recorded at $y = 0.40$ m (not presented).

It can be also noticed form Figs. 10a, d that in cross sections near the bend entrance and close to its exit the streamwise velocity at the channel centreline in the plane close to the water surface is not affected by the bend curvature.

Table 4. Dimensionless length of the maximum velocity path

Bend type	Radius / radii [m]	Location where maximum velocity path cuts the centreline (L_1 / L_b)	Location where maximum velocity path starts to follow the outer bank (L_2 / L_b)
Simple	2.6	0.314	0.668
Mild-Mild	3.3 and 2	0.295	0.549
Mild-Sharp	3.5 and 1.7	0.292	0.608
Sharp-Mild	1.7 and 3.5	0.309	0.486

3.4 EFFECT OF BEND TYPE ON BED SHEAR STRESS DISTRIBUTIONS

Bed shear stress is one of the key factors for estimation of sediment transport in rivers and open channels. The effect of bend type on dimensionless bed shear stress ($\tau_0 / \rho V^2$) for all cases is presented in Figure 12. Here V stands for the outflow cross-sectional average velocity and ρ is water density. Two regions with maximum bed shear stress are distinguished regardless the bend layout – one is located close to the end of the bend, and the other is located near the radius inflection point. High velocity gradients are the main reason for the development of the high bed-shear stress region close to the end of the bend. As it can be seen from Figure 11 these high velocity gradients result from the movement of the high velocity core towards the outer bank and its expansion towards the bed [13]. The area with

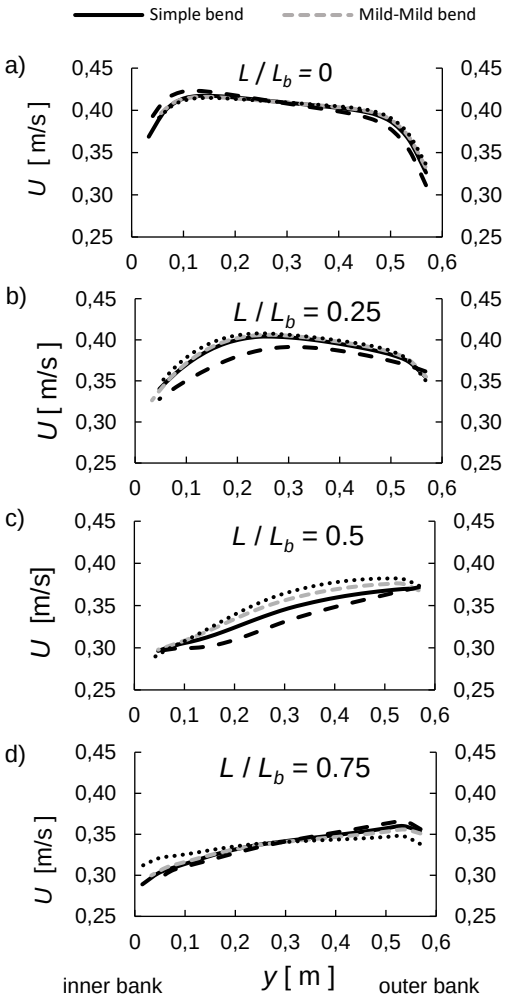

Figure. 10. Effect of bend type on lateral profiles of streamwise velocity in different cross-sections within the bend

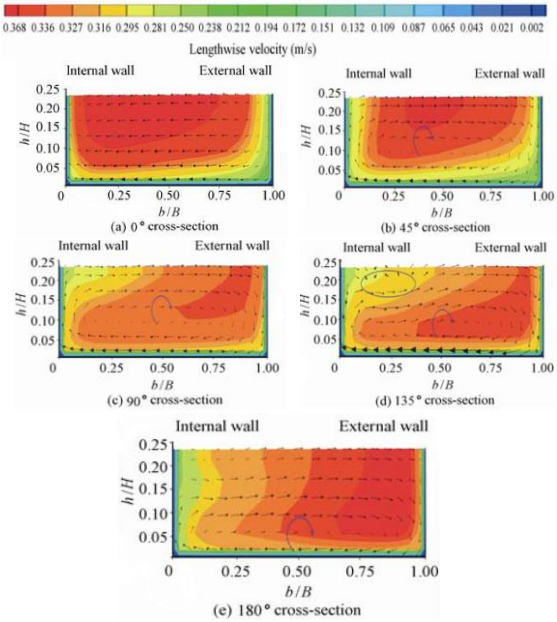

Figure. 11. Velocity distributions and secondary flows at different cross-sections in simple bend [13]

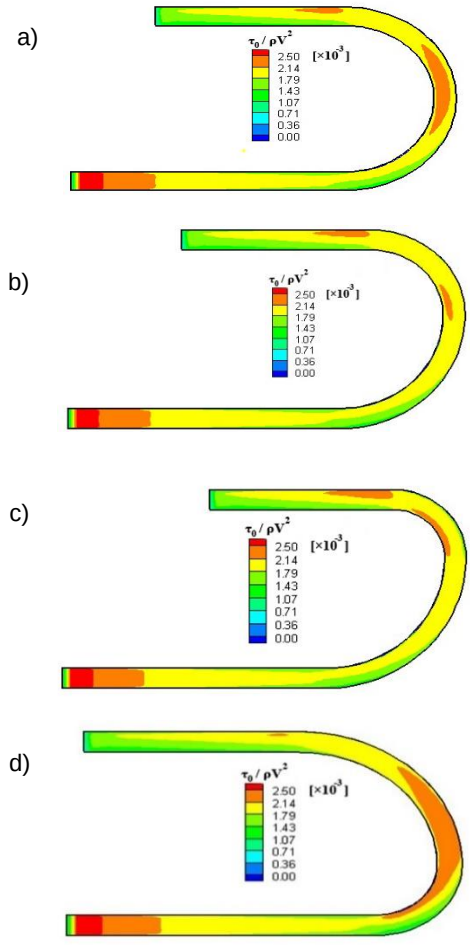

Figure 12. Effect of bend type on bed shear stress distribution: a) simple bend, b) Mild-Mild bend, c) Mild-Sharp bend and d) Sharp-Mild bend

the maximum bed shear stress close to the end of a bend is significantly reduced in the Sharp-Mild bend (by almost 90%) when compared to the simple bend. This area reduction is attributed to an increase in the second bend radius (R_2 = 3.5 m), when compared to the radius of the simple bend (R_c = 2.6 m). On the other hand, in Mild-Mild and Mild-Sharp bends decrease in the second radius, when compared to the radius of a simple bend (see Table 2), results in an increase of the $\tau_{0,\max}$ area. The percentage increase in the Mild-Mild bend is approximately 38% and in the Mild-Sharp bend, around 87%.

The size of the $\tau_{0,\max}$ area, which is located near the radius inflection point grows in Sharp-Mild bends and reduces in the Mild-Mild and Mild-Sharp bends. When compared to the size of the corresponding area in the simple bend (bend apex area), the percentage growth in the Sharp-Mild case almost reaches 180%, while percentage reductions in the Mild-Mild and Mild-Sharp bends are 81% and 76%, respectively.

4. CONCLUSIONS

The effect of bend type on flow characteristics in a 180° variable curvature channel bend was studied in this paper using the 3D finite-volume based numerical model SSIIM1, which solves Reynolds-Averaged Navier-Stokes equations. Equations are closed with the two-equation turbulence model of the k-ε type. The model was calibrated against the experimental data from the simple mild bend with θ = 180º (R_c / W = 4.33), first. Consequently, three variable curvature bend layouts with two alternating bend curvatures were analysed: Mild-Mild, Mild-Sharp and Sharp-Mild. The study has shown the following.

1. When the compound bend starts with the Mild bend of the greater radius than the simple bend, the maximal lateral slope of the water surface is less than that in the simple bend. However, the lateral slope increases right after the bend curvature transition point. The position of the cross-section with the maximal lateral slope moves downstream with the increase in downstream bend curvature.

2. When the Sharp bend precedes the Mild bend, the maximal lateral slope of the water surface is greater than that in the simple bend. However, downstream of the bend curvature

transition point, the lateral slope becomes smaller than that in a simple bend.

3. The distance from the entrance to the bend to the location where the maximum velocity path cuts the bend centreline is essentially the same regardless of the bend layout (simple or variable curvature). However, the distance to the point where the maximum velocity path starts to follow the outer bank reduces up to 27% when the sharp bend precedes the mild one.

4. The bend sequence affects lateral velocity distribution in the plane near the free-surface neither at the entrance, nor at the exit of a variable curvature bend. The differences between the four layouts exist at the bend mid-length. At this location the lowest velocity magnitudes are developed in the Sharp-Mild, and the highest velocity magnitudes in the Mild-Sharp bend. The maximal difference between the two velocity distributions is reached at $y / W = 0.40$.

5. Generally, there are two regions with the high bed shear stresses – one at the curvature inflection point and the other, close to the bend exit. When compared to the corresponding regions in the simple bend, the former one enlarges by approximately 180% when the sharp bend precedes the mild bend, and reduces by 81% and 76% as the curvature of the succeeding bend reduces. The situation with the latter one is quite the opposite – the precedence of the sharp bend causes reduction of the area size by almost 90% when compared to that in the simple bend, while precedence of the mild bend causes its growth by 38% and 87% in the Mild-Mild and Mild-Sharp bends, respectively.

REFERENCES

[1] Ahmadi, M., Ayyoubzadeh, S., M. Montazeri Namin, and Samani, J. (2009)," A 2D numerical depth-averaged model for unsteady flow in open channel bends", Journal of Agricultural Science and Technology, Vol. 11 No. 4, pp. 457-468.

[2] Akhtari, A.A., Abrishami, J. and Sharifi, M.B., (2009)," Experimental Investigations Water Surface Charachteristics in Strongly Curved Open Channels", Journal of Applied Sciences , Vol. 9 No. 20, pp. 3699-3706.

[3] Bagnold, R. A. (1960)," Some aspects of the shape of river meanders", US Government Printing Office, Pap. 282-E, Washington, D.C.

[4] Barbhuiya, A.K., and Talukdar, S. (2010)," Scour and three dimensional turbulent flow fields measured by ADV at a 90 ° horizontal forced bend in a rectangular channel", Flow measurement and Instrumentation , Vol. 21 No. 3, pp. 312-321.

[5] Blanckaert, K. (2011)," Hydrodynamic processes in sharp meander bends and their morphological implications", Journal of Geophysical Research: Earth Surface", Vol. 116 No. F01003, doi:10.1029/2010JF001806

[6] Demuren A.O., and Rodi W.(1986)," Calculation of flow and pollutant dispersion in meandering channels", Journal of fluid mechanic, Vol. 172, pp. 63-92.

[7] De Vriend, H. J., and Geldof, H. J. (1983)," Main flow velocity in short river bends", Journal of hydraulic engineering Vol. 109 No. 7, pp.991-1011.

[8] Engelund F. (1974)," Flow and bed topography in channel bends", Journal of the Hydraulics Division , Vol. 100 No. 11, pp.1631-48.

[9] Esfahani F.S. and Keshavarzi, A.R., (2010)." Experimental Study of the distribution of 3-D Velocity Components inside a Sine-Generated Sharp Open bend", 8th International River Engineering Conference, Shahid Chamran University, Ahvaz, Iran.

[10] Esfahani, F.S. and Keshavarzi, A.R. (2010)," The effect of different curvatures on flow structure inside the river meander", Ferdowsi University of Mashhad, Mashhad, Iran.

[11] Falcon M., and Kennedy J.F. (1983)," Flow in alluvial-river curves", Journal of Fluid Mechanics, Vol. 133, pp. 1-16.

[12] Fazeli, M., Ghodsian, M. and Salehi Neyshabori, A.A.S. (2008)," Scour and flow field around a spur dike in a 90° bend. International Journal of Sediment Research, Vol. 23 No. 1, pp.56-68.

[13] Ghobadian R. and Mohammadi, K. (2011)," Simulation of subcritical flow pattern in 180° uniform and convergent open-channel bends using SSIIM 3-D model", Water Science and Engineering, Vol. 4 No. 3, pp.270-283.

[14] Hickin, E. J. (1978)," Mean flow-structure in meanders of the Squamish River, British Columbia", Canadian Journal of Earth Sciences, Vol. 15 No. 11, pp.1833–1849

[15] Ikeda S., (1987)," Yamasaka M, Chiyoda M. Bed topography and sorting in bends. J Hydraul Eng ASCE, 113:190-206.

[16] Keefer, T.N. (1971)," The relation of turbulence to diffusion in open-channel flows", US Department of the Interior, Geological Survey, Water Resources Division.

[17] Leschziner, M.A. and Rodi, W. (1979)," Calculation of strongly curved open channel flow. J Hydraul Eng, 105: 1297-1314.

[18] Leeder, M. R., and Bridges P. H. (1975),"Flow separation in meander bends", Nature, Vol. 253 No. 5490, pp. 338–339, doi:10.1038/253338a0

[19] Lien H.C., Hsieh T.Y., Yang J.C., and Yeh K.C. (1995)," Bend-flow simulation using 2D depth-averaged model", Journal of Hydraulic Engineering, Vol. 125 No. 10, pp.1097-108.

[20] Liyaghat, A., Mohammadi, K. and M. Rahmanshahi. (2014),“ 3D Investigation of Flow Hydraulic in U Shape Meander Bends with Constant, Decreasing and Increasing Width“, Journal of River Engineering, Vol 3, pp. 12-23.

[21] Manssori, A.R. (2006),“ 3D Numerical Simulation of Bed Topography in 180-degree Channel Bend“, Faculty of engineering. Tarbiatmodarres University, Tehran, Iran. (Unpublished MasterThesis)

[22] Mosonyi, E. and Gotz. W. (1973),“ Secondary currents in subsequent model bends“, Proceedings of the International Association for Hydraulic Research International Symposium on River Mechanics. Jan 9-12, Asian Institute of Technology, Bangkok, pp. 191-201.

[23] Naji Abhari M., Ghodsian M., Vaghefi M. and Panahpura, N. (2010),“ Experimental and numerical simulation of flow in a 90º bend“, Flow Measurement and Instrumentation , Vol. 21 No. 3, pp.292-298.

[24] Nanson, R. A. (2010),“ Flow fields in tightly curving meander bends of low width-depth ratio“, Earth Surface Processes and Landforms, Vol. 35 No.2, pp.119–135.

[25] Nezu, I., Nakagawa, H., and Jirka, G. H. (1994),“ Turbulence in open-channel flows“, Journal of Hydraulic Engineering, Vol. 120 No.10, pp.1235-1237.

[26] Olsen, N.R.B. (2000),“ CFD algorithms for hydraulic engineering“, Trondheim: The Norwegian University of Science and Technology

[27] Olsen N.R.B., and Stokseth S. (1995),“Three-dimensional modeling of water flow in a river with large bed roughness. Journal of Hydraulic Research, Vol. 33 No.4, pp.571-81.

[28] Olsen, N.R.B. (2004),“ Hydroinformatics, fluvial hydraulics and limnology“, Department of Hydraulic and Environmental Engineering. The Norwegian University of Science and Technology.

[29] Pirestani, M. (2004),“ Study of Flow and Scouring Patterns at Intake Entrance of Curved Canals“, Azad Islamic University, Tehran, Iran. (Unpublished PhD dissertation)

[30] Rodi, W. (1980),“ Turbulence models and their application in hydraulics, CRC Press, International Association of Hydraulic Research Section.

[31] Rozovskii, I.L. (1957),“ Flow of water in bends of open channels“, Academy of Sciences of the Ukrainian SSR Institute of Hydrology and Hydraulic Engineering.

[32] Schlichting, H. (1979),“ Boundary- layer theory“, Springer Science & Business Media, McGraw-Hill New York.

[33] Shimizu Y., Yamaguchi Y., and Itakura T. (1990),“ Three-dimensional computation of flow and bed deformation. Journal of Hydraulic Engineering , Vol. 116 No. 9, pp.1090-107.

[34] Shukry, A. (1950),“ Flow around bends in an open flume. Transactions of the American Society of Civil Engineers, Vol. 115 No. 1, pp. 751-779.

[35] Stoesser, T., Ruether, N. and Olsen, N.R.B. (2010),“ Calculation of primary and secondary flow and boundary shear stresses in a meandering channel“, Advances in Water Resources, Vol. 33 No. 2, pp. 158-170.

[36] Vaghefi, M., Akbari, M. and Fiouz, A.R. (2015),“ Experimental Investigation of the three-dimensional flow velocity components in a 180 degree sharp bend. World appl program, Vol. 5 No. 9, pp. 125-131.

[37] Vaghefi, M., Ghodsian, M. and Adbi, A., (2012),“ Experimental study on the effect of froude number on temporal variation of scour around a T shaped spur dike in a 90 degree bend“, Applied Mechanics and Materials , Vol. 147, pp. 75-79.

[38] Vaghefi, M., Akbari, M., and Fiouz, A.R. (2014),“ Experimental investigation on bed shear stress distribution in a 180 degree sharp bend by using Depth-Averaged method. International Journal of Scientific Engineering and Technology (IJSET), Vol. 3 No. 7, pp. 962-965.

[39] Ye J., and McCorquodale J.A. (1998),“Simulation of curved open channel flows by 3D hydrodynamic model“, Jornal of Hydralogic Engineerng Vol. 124 No. 7, pp. 687-98.